Editors' Suggestion

Pyroelectric and electrocaloric effects in ferroelectric silicon-doped hafnium oxide thin films

Shishir Pandya,[1] Gabriel Velarde,[1] Lei Zhang,[1] and Lane W. Martin[1,2,*]

[1]*Materials Science and Engineering, University of California Berkeley, Berkeley, California 94720, USA*

[2]*Materials Sciences Division, Lawrence Berkeley National Laboratory, Berkeley, California 94720, USA*

(Received 11 September 2018; published 28 December 2018)

The emergent ferroelectricity in HfO_2-based systems has attracted significant attention as this simple binary high-k dielectric now offers the possibility of nonvolatile function. In this work we employ zero-field and field-dependent pyroelectricity to show that thin films of silicon-doped HfO_2 do exhibit a broken-inversion symmetry and are indeed ferroelectric. In addition, the pyroelectric response is found to exhibit a wake-up behavior akin to the wake-up phenomenon observed in the ferroelectric polarization with electric-field cycling. Using polarization-electric field hysteresis measurements, this wake-up phenomenon is attributed to the presence of defect dipoles which explains the measured pyroelectric response. Finally, direct electrocaloric measurements are performed on these silicon-doped HfO_2 thin films, revealing an electrocaloric coefficient ~4 times larger in magnitude than that expected for the measured pyroelectric coefficient. This enhancement is explained using the plausible role played by defect dipoles that contribute to additional configurational or dipolar entropy.

DOI: 10.1103/PhysRevMaterials.2.124405

I. INTRODUCTION

While there is increasing evidence to support the existence of intrinsic ferroelectricity in the simple binary oxide HfO_2, pyroelectricity, the requisite property that confirms a polar phase in which ferroelectricity can occur, has remained relatively unexplored. Probing the temperature-dependent changes in the spontaneous polarization (the pyroelectric effect or PEE) would, therefore, not only prove if the point-group symmetry of the crystal permits ferroelectricity [1], but also gauge the extent of the susceptibility of the polarization to any change in the temperature. Prior reports [2] using indirect measurement techniques have claimed the existence of an exorbitantly large PEE in silicon-doped HfO_2 (Si:HfO_2) which was attributed to a temperature-driven phase transition, while more recent work using a phase-sensitive detection technique [3,4] on zirconium-doped HfO_2 [5] and Si:HfO_2 [6,7] has shown that PEE in these simple fluorite structures is rather modest. Furthermore, since any pyroelectric material also exhibits the electrocaloric effect (ECE), there is growing interest to explore how much an electric field can perturb the dipolar entropy and, therefore, the temperature in this CMOS-compatible system. Recent work on zirconium-doped HfO_2 thin films, using indirect measurement techniques (which are often misleading as they are readily confounded by spurious contributions in thin films) [8], have suggested the existence of a large ECE [9]. Despite this observation, a plausible mechanism for the large values has remained elusive, calling into question the veracity of such reports. A detailed study is therefore essential to develop a deeper physical insight into the electrothermal response and to explore the potential for pyroelectric energy conversion [10,11] and electrocaloric solid-state cooling [12] in this new lead-free and CMOS-compatible ferroelectric.

HfO_2 has various polymorphs in the bulk depending on pressure and temperature. Under atmospheric pressure, temperature-induced phase transitions from a monoclinic ($P2_1/c$) to tetragonal ($P4_2/nmc$) and finally to a cubic ($Fm3m$) phase occur at 1973 and 2773 K, respectively [13]. All of these phases possess a center of inversion symmetry and are therefore nonpolar. A polar orthorhombic phase ($Pca2_1$), energetically very close to the nonpolar monoclinic phase at room temperature [14], however, can be stabilized under different mechanical [15–17] and chemical environments. First, stabilized with magnesium doping [18], different dopants including aluminum [19], gadolinium [20], lanthanum [21], silicon [22], strontium [23], and yttrium [24] have been shown to stabilize ferroelectricity in HfO_2-based systems. In the case of Si:HfO_2, the ferroelectric polarization requires a so-called "wake-up" process [25] wherein an initially constricted ferroelectric hysteresis behavior relaxes and the remnant polarization is enhanced after electric-field cycling [26]. This is analogous to the phenomena observed in $BaTiO_3$ single crystals [27,28] and $PbZr_{1-x}Ti_xO_3$ ceramics [29,30] where point defects (vacancies) can occupy energetically favorable sites in the bulk lattice [27,28], domain walls [31], or grain boundaries [32] and form defect dipoles or complexes that create a restoring force favoring a certain direction of spontaneous polarization. Recent work on thin films of Si:HfO_2 has reported the presence of defect dipoles due to nonhomogeneously aggregated oxygen vacancies that can cause the as-grown ferroelectric domains to be preferentially polarized in order to screen the internal bias field [33]. Since the pyroelectric susceptibility [$\pi_i = (\frac{\partial \langle P_i \rangle}{\partial T})_E$] strongly depends on the net polarization [$\langle P_i \rangle$], any change in $\langle P_i \rangle$ due to the presence of defects can significantly alter the pyroelectric response. Furthermore, since the defects can alter the permissible configurational states for the polarization [34,35], the additional

*lwmartin@berkeley.edu

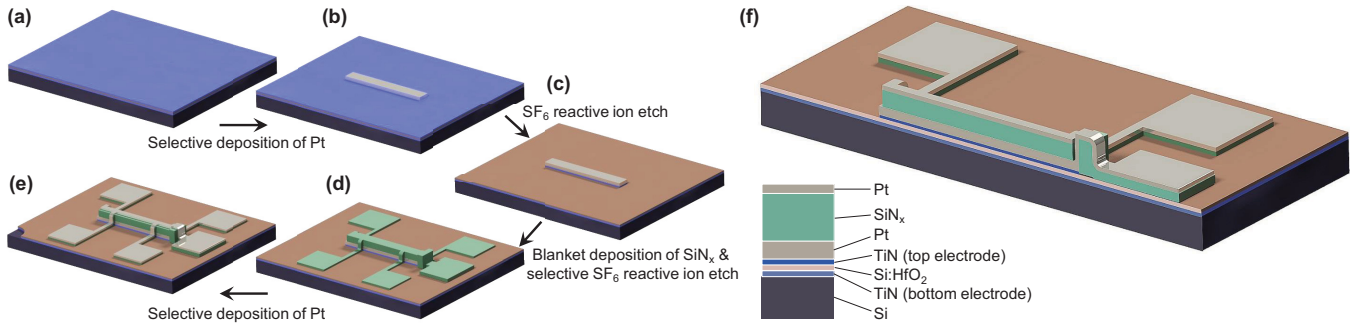

FIG. 1. (a)–(e) Schematic illustration showing the fabrication of the electrothermal device through the various processing steps. (f) Cross-section view of the final device showing the various layers in the heterostructure.

dipolar entropy change can constitute a novel mechanism for electrocaloric susceptibility [$\Sigma_i = (\frac{\partial S}{\partial E_i})_T$].

In this work we investigate the PEE and ECE in 10-nm-thick films of Si:HfO_2. High-frequency, localized heating was employed to measure the pyroelectric coefficient (π) directly using phase-sensitive detection [36]. By systematically waking up the polarization using bipolar electric-field cycling, we investigate the evolution of π. By measuring the wake-up-cycle-dependent ferroelectric-electric field hysteresis loops, the presence of defect dipoles in thin films of Si:HfO_2 is established. In turn, the role of defect dipoles in affecting π is illustrated. Finally, direct measurements are conducted to measure the electrocaloric susceptibility (Σ) in these ultra-thin Si:HfO_2 films. Comparison between π and Σ reveals a significant deviation from the Maxwell relations (Σ is more than ~4 times larger than expected for the measured value of π), suggesting that defect dipoles/complexes can potentially contribute to the high-field electrocaloric response through field-driven rearrangement.

II. DEVICE FABRICATION

Electrothermal devices were fabricated using as-received, rapid-thermal-annealed 10 nm TiN/10 nm 5.88 mol % Si:HfO_2/10 nm TiN heterostructures on a doped-silicon wafer produced in the Center for Nanoelectronic Technologies at the Fraunhofer Institute for Photonic Microsystems in Dresden, Germany (Fig. 1). The phase of the as-received films was confirmed to be orthorhombic using grazing-incidence x-ray diffraction (Supplementary Material, Fig. S1 [37]). To produce the electrothermal devices, 30 nm of platinum was first sputtered on the as-received metal-ferroelectric-metal trilayer heterostructures [Fig. 1(a)] after lithographically patterning a $300 \times 20\ \mu m^2$ rectangular top electrode [Fig. 1(b)] to enhance the electrical conductivity of an otherwise poorly conducting TiN top electrode. The unneeded top TiN was etched away (using SF_6 plasma-based reactive ion etching) using the above platinum as a hard mask from everywhere except the active device ($300 \times 20\ \mu m^2$ rectangular area) to define the ferroelectric capacitor geometry with the bottom TiN and silicon wafer serving as the bottom electrode and the platinum on the top TiN serving as the top electrode [Fig. 1(c)]. A 200-nm-thick blanket layer of SiN_x was deposited using plasma-enhanced chemical vapor deposition ($SiH_4 + NH_3$ based) and was selectively etched (using SF_6 plasma-based reactive ion etching) leaving an electrically insulating layer on the ferroelectric capacitor [Fig. 1(d)]. Finally, a 50-nm-thick layer of platinum was sputtered to define the thermal characterization circuit (akin to a four-point probe pattern) and the contact pad to access the top electrode [Fig. 1(e)]. Note that the thermal characterization circuit does not electrically short with the capacitor circuit underneath [Fig. 1(f)].

III. UNDERSTANDING THE PYROELECTRIC EFFECT IN Si-DOPED HfO_2 THIN FILMS

A. Measurement of pyroelectric susceptibility

To probe the pyroelectric response in the HfO_2 heterostructures, a 10 mA (rms) sinusoidal heating current was sourced into the microfabricated platinum heating line. 3ω measurements were conducted to estimate the resulting temperature change in the ferroelectric (Si:HfO_2) [Supplemental Material, Fig. S2(a)] [37]. Since the substrate (doped-silicon wafer) is electrically conducting, additional experiments confirming the scaling of first and third harmonics of the measured response were performed to ensure that there was no electrical crosstalk between the thermal circuit and the top/bottom electrode of the ferroelectric capacitor [Supplemental Material, Figs. S2(b) and S2(c)] [37]. For the pyroelectric measurements reported herein, the heating current at a frequency of 1 kHz (1ω) was employed. This heating current results in a temperature oscillation of 0.61 K (rms) at 2 kHz (2ω) as calculated using the measured value of the temperature coefficient of resistance of the platinum heating line. Subsequently, π is calculated using $\pi = i_p(A\frac{dT}{dt})^{-1}$ where i_p is the measured pyroelectric current and A is the area of the sinusoidally heated cross section of the device.

Polarization-electric field hysteresis loops were first measured on the as-grown device (having subjected the heterostructures to no electric-field cycles or dc bias). The as-received ferroelectric hysteresis loops reveal a distinct "pinched" characteristic [Fig. 2(a)] as has been observed in prior reports for Si:HfO_2 thin films [22,25,38,39]. This pinched or constricted hysteresis loop has often been attributed to antiferroelectric behavior in Si:HfO_2 thin films [38,40–42] in contradiction to the proposed explanations attributing the double-hysteresis behavior to the defect-induced internal bias fields [43]. The presence of either an antiferroelectric behavior or defect-induced pinning/back-switching

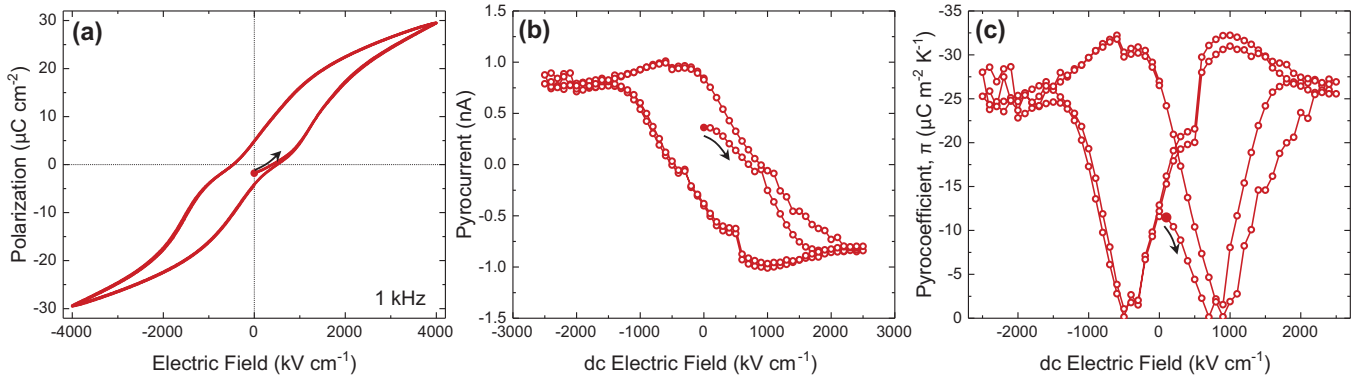

FIG. 2. (a) Polarization-electric field hysteresis loop measurements showing a pinched or constricted hysteresis loop in the as-received Si:HfO_2 films. (b) Pyroelectric current (i_p) and (c) pyrocoefficient (π) measured as a function of background dc electric field, at 1 kHz. The black arrows and filled red data point show the direction and starting point of the measurements.

of ferroelectric domains should manifest in the pyroelectric response as well. Antiferroelectric ordering should result in a zero value of π under zero bias while back-switching of ferroelectric domains due to defect pinning should result in a reduction of π below the coercive field. To investigate this phenomenon, pyroelectric measurements were conducted while sweeping the background dc electric field. It can be seen that the magnitude of both i_p [Fig. 2(b)] and π (Fig. 2(c)] under zero dc electric field (shown as a filled red circle and marked as the starting point of the field sweep using a black arrow) is nonzero confirming that the pinched hysteresis loop is not due to antiferroelectricity. As the magnitude of the dc electric field is increased, the magnitude of both i_p [Fig. 2(b)] and π [Fig. 2(c)] increases in comparison to the zero-field response. This field-induced enhancement in the magnitude of π is likely due to an increase in the net polarization due to 180° switching of ferroelectric domains. Furthermore, it should also be noted that the zero-field response of π after saturation under a high bias does not trace back along the original path (compare i_p and π under zero electric field with the starting values shown as a shaded red circle). This suggests that the switched ferroelectric domains do not completely switch back after the electric field is removed, in-turn, suggesting that the polarization in the ferroelectric has progressively woken up as the bias is applied.

The field-dependent pyroelectric measurements additionally enable the quantification of the contribution from the temperature-dependent change in the relative dielectric permittivity (ε_r). Under a background dc electric field (E) applied along the direction of polarization (z direction), π captures additional contributions which can be mathematically expressed as

$$\pi = \frac{\partial P}{\partial T} = \frac{\partial P_r}{\partial T} + \varepsilon_0 E \frac{\partial \varepsilon_r}{\partial T}, \tag{1}$$

where P is the net polarization under an electric field and P_r is the remanent polarization. Depending on the sign of $(\frac{\partial \varepsilon_r}{\partial T})$, the contribution from the temperature-dependent change in ε_r can either enhance or diminish π. This contribution is particularly important for pyroelectric energy conversion where the thermodynamic cycles usually involve temperature changes under an electric field. From the current work, it can be seen that under an applied electric field the magnitude of i_p [Fig. 2(b)] and π [Fig. 2(c)] first increases to a maximum and then starts to diminish. The initial increase is due to an increase in the degree of alignment of the ferroelectric domains which outweighs the competing contribution from the $(\varepsilon_0 E \frac{\partial \varepsilon_r}{\partial T})$ term which is positive (i.e., the permittivity increases with temperature) while the $(\frac{\partial P_r}{\partial T})$ term is negative (i.e., polarization decreases with temperature). Once the domains are aligned, further increasing the electric field results in the reduction of π since the competing contribution from the $(\varepsilon_0 E \frac{\partial \varepsilon_r}{\partial T})$ term starts to dominate π.

As shown here [Figs. 2(b) and 2(c)], the application of E enhances π due to an increase in P_r. Since the polarization can be woken up with electric-field cycling, pyroelectric measurements were conducted as a function of the number of the wake-up cycles. To achieve a systematic increase in P_r the devices were field cycled using a sinusoidal electric field with an amplitude of 4 MV cm^{-1} at a frequency of 1 kHz. The ferroelectric hysteresis loops for the as-grown state and after 2000 and 200 000 cycles are shown [red, yellow, and blue curves, respectively, Fig. 3(a)]. Immediately after the wake-up process for each number of cycles, π was measured [Fig. 3(b)]. It can be seen that both P_r and π increase with the number of electric-field cycles; P_r increases from ~5 [red data, Fig. 3(a)] to ~10 $\mu C\,cm^{-2}$ [blue data, Fig. 3(a)] and π increases from ~−13 to ~−27 $\mu C\,m^{-2}\,K^{-1}$ [dashed line shows an empirical logarithmic dependence [25], Fig. 3(b)] after 200 000 cycles. Both the pinched hysteresis loop and an imprinted hysteresis loop [Fig. 3(a)] are signatures of the presence of defect dipoles in ferroelectrics [27,44]. Therefore, the observed behavior of ferroelectric and pyroelectric susceptibility with field cycling in the current work can be attributed to the presence of defect dipoles.

B. Effect of defect dipoles on ferroelectric and pyroelectric susceptibility

In general, the term defect dipole refers to any defect complex formed out of oppositely charged point defects in a lattice that couples such that their association reduces the free energy of the system [45,46]. In ferroelectrics, such defect complexes are typically comprised of either an acceptor defect and an oxygen vacancy [26] or a donor defect and a cation vacancy [44]. Recent work on Si:HfO_2 has revealed

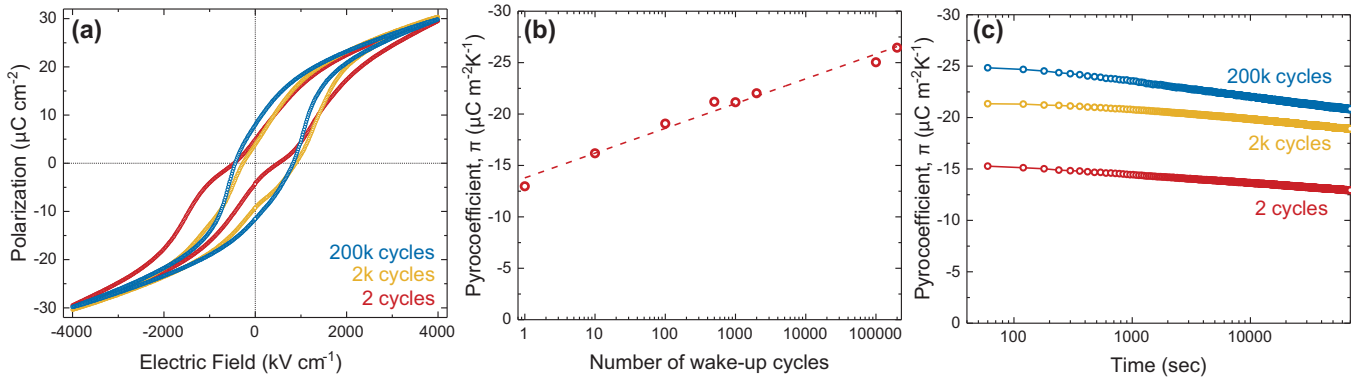

FIG. 3. (a) Polarization-electric field hysteresis loop measurements conducted after electrically cycling the device for 2 (red), 2000 (2k, yellow), and 200 000 (200k, blue) cycles. (b) Measured pyroelectric coefficient (π) as a function of the number of wake-up cycles. The red dashed line shows an empirical logarithmic fit to the measured data. (c) Pyroelectric-retention measurements conducted on samples after 2 (red), 2000 (2k, yellow), and 200 000 (200k, blue) wake-up cycles.

the presence of charged-oxygen vacancies [47] and the possibility for the formation of defect dipoles/complexes due to an interfacial chemical reaction between the HfO_2 and TaN (or TiN) [33]. The observed ferroelectric switching response can, therefore, be interpreted by considering a scenario where the defect dipoles (with a net polarization P_D) contribute to the overall polarization ($P_r = P_i + P_D$), where P_i is the intrinsic polarization of Si:HfO_2. Since the dipolar interaction between the defect dipoles and the intrinsic polarization in the lattice energetically favors a parallel alignment of P_D and P_i [27,44,45], a much smaller measured value of P_r in the as-grown state [red data, Fig. 3(a)] indicates that the defect dipoles have a near-equal probability of pointing up and down. Consequently, a certain fraction of P_i within the range of interaction with the defect dipole remains coupled or prefers to remain aligned parallel with P_D.

During a single ferroelectric switching process, the defects do not switch due to their slower migration kinetics. In turn, they provide a restoring force to the adjacent intrinsic polarization that had switched under the applied electric field, to back-switch once the field is removed causing a pinched hysteresis loop [27]. The near-equal distribution of the up- and down-pointing defect dipoles causes the net built-in potential across the ferroelectric to be zero and therefore there is a negligible horizontal offset or imprint [red data, Fig. 3(a)]. After repeatedly electrical cycling of the ferroelectric, however, the as-grown defect orientation can be altered. The imprint in the measured ferroelectric hysteresis loops after 200 000 cycles [blue data, Fig. 3(a)] is indicative of a net nonzero built-in potential across the ferroelectric suggesting that the probability of the up- and the down-pointing defect dipoles is no longer equal and that the defect dipoles are now largely pointing in a single preferred direction. A positive horizontal offset along the electric-field axis indicates that under zero applied electric field, an up pointing or $-P_r$ state is favored. Back-switching now happens after poling the ferroelectric in the $+P_r$ state only. Consequently, the pinching in the ferroelectric hysteresis loop is reduced. The pyroelectric susceptibility, likewise, shows an increase as P_r increases [Fig. 3(b)].

To check the stability of the pyroelectric response after the polarization wake-up process, pyroelectric-retention measurements were conducted. Here, after poling the ferroelectric in the up-poled state with a bipolar triangular pulse after a varying number of wake-up cycles, π was measured as a function of time [Fig. 3(c)]. It can be seen that π decreases with time for all cases of wake-up cycling [2, 2000, and 200 000 cycles shown in red, yellow, and blue color, respectively, Fig. 3(c)]. This suggests that the up-pointing alignment of the defect dipoles slowly relaxes back to the state where some of the defect dipoles have switched to be down pointing with time. Additional retention measurements were performed with the polarization switched in the down-poled direction (Supplemental Material, Fig. S3 [37]). Here also, the decrease in π with time for all the cases of wake-up cycling suggests that the defect dipoles relax back into a state where some of the defect dipoles switch back.

IV. UNDERSTANDING THE ELECTROCALORIC EFFECT IN Si-DOPED HfO_2 THIN FILMS

A. Measurement of electrocaloric susceptibility

Armed with an understanding of the PEE in Si:HfO_2, we proceed to investigate ECE in the same thin films. Using the same device structures as for measuring the PEE, ECE measurements were conducted by applying an ac electric field to measure the electrocaloric-temperature change. Briefly, a sinusoidally varying electric field was applied across the ferroelectric heterostructure at 98.147 kHz. In response to the ac electric-field perturbation, the resulting sinusoidal temperature oscillation in the ferroelectric was measured using an ac sensing current with a magnitude of 2 mA at a frequency of 2.317 kHz applied across the top line. The electrocaloric response (manifested as an ac voltage) was measured at $98.147 - 2.317 = 95.830$ kHz. Using the temperature coefficient of resistance, the ac temperature change in the top metal line (θ_{Sensor}) was calculated and subsequently used to calculate Σ after solving the 1D heat transport model using the thermophysical properties of the heterostructure (Table I).

Beginning with the as-grown heterostructures [exhibiting ferroelectric hysteresis loop response shown as red data, Fig. 3(a)], the temperature of the top metal line θ_{Sensor} was measured as a function of increasing ac electric-field

TABLE I. Thermophysical properties (at 300 K) of the various thin films and substrates used in the thermal transport calculations.

Film/substrate	Thermal conductivity k (W m^{-1} K^{-1})	Specific heat capacity $C(T)$ (J m^{-3} K^{-1})
Si:HfO_2	1.0[a]	2.76×10^{6}[b]
TiN	2.7[c]	3.47×10^{6}[c]
SiN_x	2.0[d]	1.16×10^{6}[e]
Si	120[f]	Assumed as 1.6×10^{6}[f]

[a]Reference [48].
[b]Reference [49].
[c]Reference [50].
[d]Reference [36].
[e]Reference [51].
[f]Reference [52].

perturbation. The maximum bipolar electric field applied to perturb the entropy of the system was limited to 1.25 MV cm^{-1}. This was done for two reasons: (1) to ensure that the ferroelectric does not switch and (2) to ensure that the polarization in the ferroelectric is not woken up by applying a bipolar electric field. It can be seen that θ_{Sensor} scales linearly with the applied electric field [red squares, Fig. 4(a)]. Using a thermal transport model and various values of material parameters (Table I) [36], Σ was calculated [filled red circles, Fig. 4(a)]. Next, the sample was cycled with electric field 2000 times to wake up the polarization [see ferroelectric hysteresis loop shown in yellow, Fig. 3(a)]. Similar to the as-grown sample, θ_{Sensor} scaled linearly [yellow squares, Fig. 4(a)] with the applied ac electric field while Σ remained field independent [filled yellow circles, Fig. 4(a)]. Finally, the same sample was subjected to 200 000 electric field wake-up cycles [see ferroelectric hysteresis loop shown in blue, Fig. 3(a)] and θ_{Sensor} [blue squares, Fig. 4(a)] and Σ [filled blue circles, Fig. 4(a)] were again measured. It can be seen that Σ does not change with repeated electric-field cycling; unlike the effect seen for π.

In general, for ferroelectrics with 180° domain structures, the domains where the spontaneous polarization is aligned with the electric field exhibit conventional ECE (application of field reduces the dipolar entropy or increases the lattice temperature) while the domains where the polarization is anti-aligned with the applied electric field exhibit an inverse ECE (application of field increases the dipolar entropy or decreases the lattice temperature) [36]. In the current scenario, the as-grown sample exhibits a reduced value of P_r suggesting the presence of near-equal magnitude of up- and down-pointing polarization. Therefore, the ECE for such a case should exhibit a much lower value than measured. As such, the ECE should have increased with the number of wake-up cycles, but in the current case ECE remains independent of the number of wake-up cycles. Again, this is in sharp contrast to π which steadily increases as P_r increases [Fig. 4(b)]. Additionally, the magnitude of Σ is ~4 times larger than what is expected for the measured value of π. Based on the Maxwell's equation that relates π and Σ under a constant-stress boundary condition, and the fact that one would expect values of π to be higher than values of Σ for mechanically clamped thin films [53], the results (Fig. 4) suggest that the ECE very likely involves additional contributions to the change in the entropy. We propose the deviation arises from the presence of the defect dipoles.

B. Effect of defect dipoles on electrocaloric susceptibility

In the case of an equal distribution of up- and down-pointing defect dipoles (as in the case of the as-grown heterostructures with pinched ferroelectric hysteresis loops), the ensemble of polarization configurations is larger than what would occur in a homogeneously poled ferroelectric; thus that system would have the potential for higher configurational entropy. Under the application of an electric field, the intrinsic polarization is poled along the direction of the applied electric field thus reducing the dipolar entropy. As the field is removed/reversed (without a net switching of the

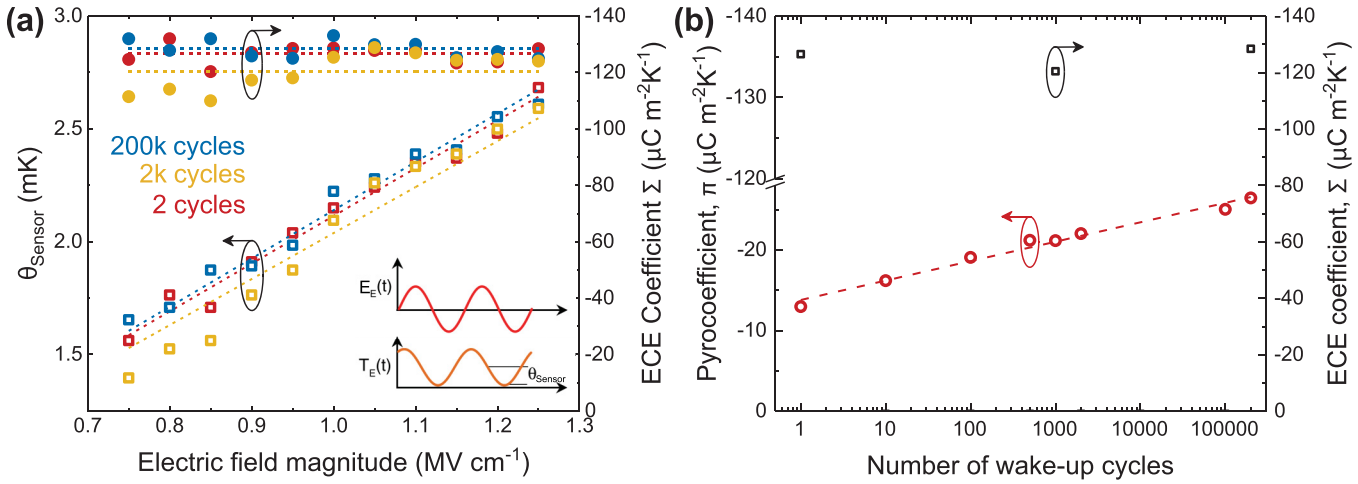

FIG. 4. (a) Measured temperature change of the top metal line (θ_{Sensor}; open squares, left axis) and the calculated value of the electrocaloric coefficient (Σ) (filled circles, right axis) on devices after 2 (red), 2000 (2k, yellow), and 200 000 (200k, blue) wake-up cycles. The inset shows the schematic of the phase relationship between the applied electric field and the temperature. (b) Comparison of π (red circles, left axis) with Σ (black squares, right axis) as a function of the number of wake-up cycles.

ferroelectric), the back-switching of some fraction of the intrinsic polarization makes the system configurationally disordered again resulting in a higher ECE in comparison to a case where the polarization would not have back-switched. Thus, in the presence of defect dipoles with a propensity to point equally in both the directions, the entropy under a zero-field state is higher than the case if there is no additional disorder imposed by the defect dipoles. Next, when the defect dipoles are largely aligned to point in the same direction after the wake-up cycles [in the case of the heterostructure with an unpinched, but imprinted ferroelectric hysteresis loop, blue data in Fig. 3(a)], application of electric field again aligns the intrinsic polarization along the direction of an applied electric field. As the electric field is removed/reversed, however, a significant fraction of the intrinsic polarization back-switches again making the dipolar state more disordered than a scenario where there exists no back-switching. Thus, in both the cases, the presence of defect dipoles provides more configurations in the zero-field state causing additional entropy changes.

V. CONCLUSION

To summarize, the pyroelectric and electrocaloric response was investigated in 10-nm-thick Si:HfO_2 films. Pyroelectric measurements support the existence of ferroelectricity which was evident from the switching of polarity of the pyroelectric current. Field-dependent pyroelectric measurements additionally provide the magnitude of the contribution from the temperature-dependent change in the dielectric permittivity. By measuring the ferroelectric susceptibility as a function of wake-up cycles, the presence of defect dipoles is suggested. In turn, the wake-up phenomenon exhibited in the pyroelectric response was explained. Finally, direct electrocaloric measurements were conducted on HfO_2-based thin films. The measured values of the electrocaloric coefficient were found to be ∼4 times larger in magnitude in comparison to its thermodynamic-converse pyroelectric coefficient. The enhancement in the ECE is explained using the plausible role played by defect dipoles that contribute to additional configuration or dipolar entropy.

ACKNOWLEDGMENTS

The authors acknowledge Thomas Kampfe and Patrick Polakowski from Fraunhofer IPMS, Dresden, Germany for providing the Si:doped HfO_2 samples studied in this work. S.P. acknowledges support from the Army Research Office under Grant W911NF-14-1-0104. G.V. acknowledges support from the National Science Foundation under Grant No. DMR-1708615. L.Z. acknowledges support from the U.S. Department of Energy, Office of Science, Office of Basic Energy Sciences, under Award Number DE-SC-0012375 for the study of ferroelectric thin films. L.W.M. acknowledges partial support from the U.S. Department of Energy, Office of Science, Office of Basic Energy Sciences, Materials Sciences and Engineering Division under Contract No. DE-AC02-05-CH11231 (Materials Project program KC23MP) for the development of novel functional materials.

[1] M. E. Lines and A. M. Glass, *Principles and Applications of Ferroelectrics and Related Materials* (Oxford University Press, Oxford, 1977).

[2] M. Hoffmann, U. Schroeder, C. Künneth, A. Kersch, S. Starschich, U. Böttger, and T. Mikolajick, Ferroelectric phase transitions in nanoscale HfO_2 films enable giant pyroelectric energy conversion and highly efficient supercapacitors, Nano Energy **18**, 154 (2015).

[3] L. E. Garn and E. J. Sharp, Use of low-frequency sinusoidal temperature waves to separate pyroelectric currents from non-pyroelectric currents. Part I. Theory, J. Appl. Phys. **53**, 8974 (1982).

[4] E. J. Sharp and L. E. Garn, Use of low-frequency sinusoidal temperature waves to separate pyroelectric currents from non-pyroelectric currents. Part II. Experiment, J. Appl. Phys. **53**, 8980 (1982).

[5] S. W. Smith, A. R. Kitahara, M. A. Rodriguez, M. D. Henry, M. T. Brumbach, and J. F. Ihlefeld, Pyroelectric response in crystalline hafnium zirconium oxide ($Hf_{1-x}Zr_xO_2$) thin films, Appl. Phys. Lett. **110**, 072901 (2017).

[6] S. Jachalke, T. Schenk, M. H. Park, U. Schroeder, T. Mikolajick, H. Stöcker, E. Mehner, and D. C. Meyer, Pyroelectricity of silicon-doped hafnium oxide thin films, Appl. Phys. Lett. **112**, 142901 (2018).

[7] C. Mart, T. Kämpfe, S. Zybell, and W. Weinreich, Layer thickness scaling and wake-up effect of pyroelectric response in Si-doped HfO_2, Appl. Phys. Lett. **112**, 052905 (2018).

[8] Y. Liu, J. F. Scott, and B. Dkhil, Direct and indirect measurements on electrocaloric effect: Recent developments and perspectives, Appl. Phys. Rev. **3**, 031102 (2016).

[9] M. H. Park, H. J. Kim, Y. J. Kim, T. Moon, K. D. Kim, Y. H. Lee, S. D. Hyun, and C. S. Hwang, Giant negative electrocaloric effects of $Hf_{0.5}Zr_{0.5}O_2$ thin films, Adv. Mater. **28**, 7956 (2016).

[10] S. Pandya, J. Wilbur, J. Kim, R. Gao, A. Dasgupta, C. Dames, and L. W. Martin, Pyroelectric energy conversion with large energy and power density in relaxor ferroelectric thin films, Nat. Mater. **17**, 432 (2018).

[11] R. B. Olsen, Ferroelectric conversion of heat to electrical energy: A demonstration, J. Energy **6**, 91 (1982).

[12] R. Ma, Z. Zhang, K. Tong, D. Huber, R. Kornbluh, Y. S. Ju, and Q. Pei, Highly efficient electrocaloric cooling with electrostatic actuation, Science **357**, 1130 (2017).

[13] X. Zhao and D. Vanderbilt, First-principles study of structural, vibrational, and lattice dielectric properties of hafnium oxide, Phys. Rev. B **65**, 233106 (2002).

[14] T. D. Huan, V. Sharma, G. A. Rossetti, Jr., and R. Ramprasad, Pathways towards ferroelectricity in hafnia, Phys. Rev. B **90**, 064111 (2014).

[15] H. Arashi, Pressure-induced phase transformation of HfO_2, J. Am. Ceram. Soc. **75**, 844 (1992).

[16] P. Polakowski and J. Müller, Ferroelectricity in undoped hafnium oxide, Appl. Phys. Lett. **106**, 232905 (2015).

[17] J. Müller, T. S. Böscke, U. Schröder, S. Mueller, D. Bräuhaus, U. Böttger, L. Frey, and T. Mikolajick, Ferroelectricity in simple binary ZrO_2 and HfO_2, Nano Lett. **12**, 4318 (2012).

[18] C. J. Howard, E. H. Kisi, and O. Ohtaka, Crystal structures of two orthorhombic zirconias, J. Am. Ceram. Soc. **74**, 2321 (1991).

[19] S. Mueller, J. Mueller, A. Singh, S. Riedel, J. Sundqvist, U. Schroeder, and T. Mikolajick, Incipient ferroelectricity in Al-doped HfO_2 thin films, Adv. Funct. Mater. **22**, 2412 (2012).

[20] S. Mueller, C. Adelmann, A. Singh, S. Van Elshocht, U. Schroeder, and T. Mikolajick, Ferroelectricity in Gd-doped HfO_2 thin films, ECS J. Solid State Sci. Technol. **1**, N123 (2012).

[21] M. G. Kozodaev, A. G. Chernikova, E. V. Korostylev, M. H. Park, U. Schroeder, C. S. Hwang, and A. M. Markeev, Ferroelectric properties of lightly doped La: HfO_2 thin films grown by plasma-assisted atomic layer deposition, Appl. Phys. Lett. **111**, 132903 (2017).

[22] D. Martin, J. Müller, T. Schenk, T. M. Arruda, A. Kumar, E. Strelcov, E. Yurchuk, S. Müller, D. Pohl, U. Schröder *et al.*, Ferroelectricity in Si-doped HfO_2 revealed: A binary lead-free ferroelectric, Adv. Mater. **26**, 8198 (2014).

[23] T. Schenk, S. Mueller, U. Schroeder, R. Materlik, A. Kersch, M. Popovici, C. Adelmann, S. Van Elshocht, and T. Mikolajick, Strontium doped hafnium oxide thin films: Wide process window for ferroelectric memories, in *2013 Proceedings of the European Solid-State Device Research Conference (ESSDERC)* (IEEE, Bucharest, Romania, 2013), pp. 260–263.

[24] J. Müller, U. Schröder, T. S. Böscke, I. Müller, U. Böttger, L. Wilde, J. Sundqvist, M. Lemberger, P. Kücher, T. Mikolajick *et al.*, Ferroelectricity in yttrium-doped hafnium oxide, J. Appl. Phys. **110**, 114113 (2011).

[25] D. Zhou, J. Xu, Q. Li, Y. Guan, F. Cao, X. Dong, J. Müller, T. Schenk, and U. Schröder, Wake-up effects in Si-doped hafnium oxide ferroelectric thin films, Appl. Phys. Lett. **103**, 192904 (2013).

[26] K. Carl and K. H. Hardtl, Electrical after-effects in $Pb(Ti,Zr)O_3$ ceramics, Ferroelectrics **17**, 473 (1977).

[27] X. Ren, Large electric-field-induced strain in ferroelectric crystals by point-defect-mediated reversible domain switching, Nat. Mater. **3**, 91 (2004).

[28] L. X. Zhang and X. Ren, *In situ* observation of reversible domain switching in aged Mn-doped $BaTiO_3$ single crystals, Phys. Rev. B **71**, 174108 (2005).

[29] J. Glaum, Y. A. Genenko, H. Kungl, L. Ana Schmitt, and T. Granzow, De-aging of Fe-doped lead-zirconate-titanate ceramics by electric field cycling: 180 vs. non-180 domain wall processes, J. Appl. Phys. **112**, 034103 (2012).

[30] M. Kohli, P. Muralt, and N. Setter, Removal of 90 domain pinning in $(100)Pb(Zr_{0.15}Ti_{0.85})O_3$ thin films by pulsed operation, Appl. Phys. Lett. **72**, 3217 (1998).

[31] W. L. Warren, D. Dimos, B. A. Tuttle, R. D. Nasby, and G. E. Pike, Electronic domain pinning in $Pb(Zr,Ti)O_3$ thin films and its role in fatigue, Appl. Phys. Lett. **65**, 1018 (1994).

[32] J.-S. Lee and S.-K. Joo, Analysis of grain-boundary effects on the electrical properties of $Pb(Zr,Ti)O_3$ thin films, Appl. Phys. Lett. **81**, 2602 (2002).

[33] P. D. Lomenzo, Q. Takmeel, C. Zhou, C. M. Fancher, E. Lambers, N. G. Rudawski, J. L. Jones, S. Moghaddam, and T. Nishida, Tan interface properties and electric field cycling effects on ferroelectric Si-doped HfO_2 thin films, J. Appl. Phys. **117**, 134105 (2015).

[34] Y. B. Ma, A. Grünebohm, K. C. Meyer, K. Albe, and B. X. Xu, Positive and negative electrocaloric effect in $BaTiO_3$ in the presence of defect dipoles, Phys. Rev. B **94**, 094113 (2016).

[35] A. Grünebohm and T. Nishimatsu, Influence of defects on ferroelectric and electrocaloric properties of $BaTiO_3$, Phys. Rev. B **93**, 134101 (2016).

[36] S. Pandya, J. D. Wilbur, B. Bhatia, A. R. Damodaran, C. Monachon, A. Dasgupta, W. P. King, C. Dames, and L. W. Martin, Direct measurement of pyroelectric and electrocaloric effects in thin films, Phys. Rev. Appl. **7**, 034025 (2017).

[37] See Supplemental Material at http://link.aps.org/supplemental/10.1103/PhysRevMaterials.2.124405 for calculating temperature change using the 3ω method.

[38] F. Ali, X. Liu, D. Zhou, X. Yang, J. Xu, T. Schenk, J. Müller, U. Schroeder, F. Cao, and X. Dong, Silicon-doped hafnium oxide anti-ferroelectric thin films for energy storage, J. Appl. Phys. **122**, 144105 (2017).

[39] C. Richter, T. Schenk, M. H. Park, F. A. Tscharntke, E. D. Grimley, J. M. LeBeau, C. Zhou, C. M. Fancher, J. L. Jones, T. Mikolajick *et al.*, Si doped hafnium oxide-a "fragile" ferroelectric system, Adv. Electron. Mater. **3**, 1700131 (2017).

[40] M. H. Park, Y. H. Lee, H. J. Kim, Y. J. Kim, T. Moon, K. D. Kim, J. Müller, A. Kersch, U. Schroeder, T. Mikolajick *et al.*, Ferroelectricity and antiferroelectricity of doped thin HfO_2-based films, Adv. Mater. **27**, 1811 (2015).

[41] J. Müller, P. Polakowski, S. Mueller, and T. Mikolajick, Ferroelectric hafnium oxide based materials and devices: Assessment of current status and future prospects, ECS J. Solid State Sci. Technol. **4**, N30 (2015).

[42] T. S. Böscke, J. Müller, D. Bräuhaus, U. Schröder, and U. Böttger, Ferroelectricity in hafnium oxide thin films, Appl. Phys. Lett. **99**, 102903 (2011).

[43] T. Schenk, M. Hoffmann, J. Ocker, M. Pešić, T. Mikolajick, and U. Schroeder, Complex internal bias fields in ferroelectric hafnium oxide, ACS Appl. Mater. Interfaces **7**, 20224 (2015).

[44] G. E. Pike, W. L. Warren, D. Dimos, B. A. Tuttle, R. Ramesh, J. Lee, V. G. Keramidas, and J. T. Evans, Jr., Voltage offsets in $(Pb,La)(Zr,Ti)O_3$ thin films, Appl. Phys. Lett. **66**, 484 (1995).

[45] G. Arlt and H. Neumann, Internal bias in ferroelectric ceramics: Origin and time dependence, Ferroelectrics **87**, 109 (1988).

[46] D. Damjanovic, Ferroelectric, dielectric and piezoelectric properties of ferroelectric thin films and ceramics, Rep. Prog. Phys. **61**, 1267 (1998).

[47] F. P. G. Fengler, R. Nigon, P. Muralt, E. D. Grimley, X. Sang, V. Sessi, R. Hentschel, J. M. LeBeau, T. Mikolajick, and U. Schroeder, Analysis of performance instabilities of hafnia-based ferroelectrics using modulus spectroscopy and thermally stimulated depolarization currents, Adv. Electron. Mater. **4**, 1700547 (2018).

[48] M. A. Panzer, M. Shandalov, J. A. Rowlette, Y. Oshima, Y. W. Chen, P. C. McIntyre, and K. E. Goodson, Thermal properties of ultrathin hafnium oxide gate dielectric films, IEEE Electron Device Lett. **30**, 1269 (2009).

[49] S. S. Todd, Heat capacities at low temperatures and entropies at 298.16 K of hafnium dioxide and hafnium tetrachloride, J. Am. Chem. Soc. **75**, 3035 (1953).

[50] A. A. Irudayaraj, R. Srinivasan, P. Kuppusami, E. Mohandas, S. Kalainathan, and K. Ramachandran, Photoacoustic measurement of thermal properties of tin thin films, J. Mater. Sci. **43**, 1114 (2008).

[51] B. L. Zink and F. Hellman, Specific heat and thermal conductivity of low-stress amorphous Si-N membranes, Solid State Commun. **129**, 199 (2004).

[52] H. R. Shanks, P. D. Maycock, P. H. Sidles, and G. C. Danielson, Thermal conductivity of silicon from 300 to 1400 K, Phys. Rev. **130**, 1743 (1963).

[53] T. Tong, J. Karthik, R. V. K. Mangalam, L. W. Martin, and D. G. Cahill, Reduction of the electrocaloric entropy change of ferroelectric $PbZr_{1-x}Ti_xO_3$ epitaxial layers due to an elastocaloric effect, Phys. Rev. B **90**, 094116 (2014).